TISSUE ENGINEERING: Part A
Volume 14, Number 7, 2008

DOI: 10.1089/ten.tea.2007.0279

Nanoscale Variation of Bioadhesive Substrates as a Tool for Engineering of Cell Matrix Assembly

RAM I. SHARMA, Ph.D.,[1,§] DAVID I. SHREIBER, Ph.D.,[2] and PRABHAS V. MOGHE, Ph.D.[1,2]

ABSTRACT

Although molecular and physical mechanisms of fibroblast matrix assembly have been widely investigated, the role of adhesive ligand presentation on matrix assembly has only been recently probed (Pereira *et al.* Tissue Eng., 2007). In the present study, various-sized albumin-derived nanocarriers (ANCs) were fabricated as nanoscale organization units for functionalization with the cell adhesion domain of fibronectin. The adhesion, morphology, and matrix assembly of human dermal fibroblasts were compared on substrate-deposited, ligand-ANCs of varying size. At early time points, fibroblast attachment, stress fiber formation, and spreading were higher on functionalized, larger-sized carriers than on smaller carriers. Matrix assembly was greatest at the highest ligand density on larger nanocarriers but was undetectable at the same ligand density on smaller carriers. Tracking of fluorophore-encapsulated ANCs showed that larger carriers were displaced less than smaller carriers and that atomic force microscopy of ligand-ANCs binding to adherent cells demonstrated that the larger ligand-ANCs required larger dissociation forces. Taken together, these data suggest that the greater inertia of larger adhesive nanocarriers may generate more cellular tension, which in turn, promotes up-regulation of matrix assembly. Thus, the size of the nanocarrier and the density of ligand on that nanocarrier combine to dictate the early kinetics of fibroblast matrix assembly. These insights may be useful for understanding cell–matrix interactions, as well as for development of bioactive materials with defined cell-adhesive activities such as wound repair and matrix remodeling events.

INTRODUCTION

PROPER REPAIR of tissue after injury depends on correct wound healing, a multistage process that involves different cell types for each step.[1,2] Wound healing is characterized by three overlapping phases: inflammation, tissue formation, and tissue remodeling.[3,4] One key event during tissue formation involves fibroblasts invading the wound space composed largely of fibrin and fibronectin, termed the provisional matrix.[5–7] Once the fibroblasts populate the wound site, they produce a provisional secondary extracellular matrix, consisting primarily of fibronectin, tenascin, and hyaluronan,[8–10] which begins the formation of granulation tissue. This newly synthesized secondary matrix directs repair by supporting and regulating functions of cells recruited to the wound site including cell proliferation, migration, and angiogenesis.[11] Eventually, collagen is deposited and the new matrix is further remodeled and contracted.[12]

Given the critical role that fibroblasts play in creating the matrix, it is important to understand what drives fibronectin secretion and assembly of fibrils. The provisional matrix initially used by fibroblasts can have a positive or negative effect on their ability to function. Growth factors and provisional matrix proteins guide the migration of fibroblasts into the wound bed,[13,14] where fibroblasts secrete and assemble new fibronectin-rich matrix.[15] Fibrillar fibronectin

[1]Department of Chemical and Biochemical Engineering, Rutgers University, Piscataway, New Jersey.
[2]Department of Biomedical Engineering, Rutgers University, Piscataway, New Jersey.
[§]Current affiliation: Orthopedic Biomechanics Laboratory, Universität Zürich, Zürich, Switzerland.

assembly depends on fibronectin–integrin interactions.[16] First, the α5β1 integrin receptor binds to fibronectin at the III_{9-10} cell-binding site encompassing the synergy sequence located in the 9th type III repeat[17,18] and the adjacent arginine-glycine-aspartate (RGD) cell-binding sequence in the 10th type III repeat.[19,20] This interaction induces molecular events that reorganize the actin cytoskeleton and activate signaling complexes, leading to the elongation and stretching of fibronectin from its compact form. Finally, fibronectin–fibronectin interactions lead to fibril formation.

The cytoskeleton plays a critical role during matrix assembly. Activation of Rho GTPases stimulates actin filament reorganization and fibronectin fibril formation.[21] Biochemical approaches have been used to modulate the cytoskeleton to promote assembly of fibronectin fibrils. Serum-containing medium, as opposed to serum-free media, has been shown to promote matrix assembly because of the multiple cues, such as growth factors, soluble fibronectin, and lysophosphatidic acid,[22–25] and addition of microtubule-destabilizing agents to medium, such as nocodazole, promotes stress fibers and contraction.[24] Fibroblasts also respond to spatial and mechanical inputs from substrate dimensionality and rigidity by changes in cell contractility and matrix assembly.[26–28] In these studies, cell-associated matrix assembly was greater in three-dimensional substrates than in two-dimensional substrates. The degree of rigidity of the substrate, which influences the ability of the cell to contract the substrate, has been shown to play a role in matrix assembly, where rigid substrates promote better cell attachment, and allow the cells to elongate and contract, leading to greater quantities of matrix assembly than with compliant substrates. We recently showed that the organization of cell-adhesive nanoscale carriers promotes integrin-mediated fibronectin matrix assembly through a mechanism that depends on nanocarrier surface mobility.[29] In the present work, we explored the albumin-derived nanocarrier (ANC) properties that regulate fibronectin matrix assembly. We hypothesized that, although the presentation of the extracellular ligand on the nanocarrier would modify the display and overall organization of the ligand, varying the size of the nanocarrier would result in different levels of cytoskeletal tension, which would lead to different degrees of matrix assembly. Our results identify the optimal nanocarrier size and ligand display parameters to promote cell attachment events and enhance matrix assembly. Such nanoscale interfaces can be an effective platform to alter the presentation of ligands and enhance ligand-based activation of the matrix remodeling that accompanies wound healing.

MATERIALS AND METHODS

Preparation, purification, and characterization of ANCs

ANCs were fabricated and functionalized as previously described.[30] Human serum albumin (30% (w/v); Sigma, St. Louis, MO) was diluted to 1% with phosphate buffered saline (PBS) and passed through a 0.22-μm filter (Fisher, Pittsburgh, PA) to remove potential aggregates of albumin. The pH of the albumin solution was raised to 10.65 with 0.1 N sodium hydroxide and heated to 80°C for 10 min. After cooling to 25°C in an ice bath, the solution was kept at room temperature for 10 min and the pH lowered to 6.04 with 0.1 N hydrochloric acid. The albumin solution was heated to 37°C and stirred to allow the self-assembly of albumin chains through intermolecular disulfide bonding.[31,32] Further reaction and aggregation were stopped by deactivating the remaining thiol groups by incubating with 0.1% (w/v) iodoacetamide (Sigma) for 1 h at room temperature. Monomeric albumin (66 kDa) was removed from the preparation using dialysis (molecular weight cut-off (MWCO) 100 kDa) against PBS. The buffer was changed twice after 2 h before final dialysis at 4°C overnight. After recovery from dialysis, albumin aggregates larger than 200 nm were removed from nanocarrier preparations by passage through a 0.2 μm filter. To characterize the kinetics of formation, samples were taken after 5, 10, 15, and 20 min of stirring at 37°C and analyzed using dynamic light scattering and atomic force microscopy. A PSS Nicomp 380 submicron particle sizer instrument (Santa Barbara, CA) with an argon ion laser at 532 nm was used for dynamic light scattering analysis.

Preparation of ligand-conjugated albumin nanocarriers

Glutathione-S-transferase (GST) fusion protein (the GST-$FNIII_{9-10}$ fragment) was prepared, purified, and conjugated using bioconjugation methods previously described by us.[29,30] Briefly, the protein was synthesized by transforming *Escherichia coli* cells transformed with the GST-$FNIII_{9-10}$ construct, and fusion proteins were separated from bacterial lysates using glutathione–sepharose affinity chromatography (GE Healthcare, Piscataway, NJ) following the manufacturer's recommendations. GST-$FNIII_{9-10}$ fragments and the various sized ANCs (1 mg and 2 mg, respectively) were separately reacted with N-succinimidyl 3-(2-pyridyldithio)-propionate, and the by-products of the reaction were removed using dialysis (MWCO 6 kDa) against PBS. Next, dithiothreitol (DTT) was added to the recombinant fragment and purified from excess DTT using dialysis (MWCO 6 kDa). Total protein recovered from dialysis was quantified for the ANC and the GST-$FNIII_{9-10}$ fragment using bicinchoninic acid protein assay (Pierce, Rockford, IL). Finally, 100 μg of reactive nanocarrier of various sizes (30, 50, 100, and 125 nm ANC-pyridyl disulfide (PD)) and varying mass of ligand-SH (1, 10, or 100 μg) were incubated together at room temperature for 6 h to conjugate the GST-$FNIII_{9-10}$ fragment to the surface of the carrier. Excess GST-$FNIII_{9-10}$ fragment not consumed in the conjugation reaction was removed from the conjugation products using dialysis (MWCO 100 kDa) against PBS.

Interfacial characterization of GST- FNIII$_{9\text{-}10}$–ANC adsorbed on substrates

Levels of GST-FNIII$_{9\text{-}10}$ conjugated to ANC were determined using enzyme-linked immunosorbent assay (ELISA). An ELISA for albumin was performed simultaneously for normalization of GST-FNIII$_{9\text{-}10}$ levels. Briefly, GST-FNIII$_{9\text{-}10}$–ANC and standards of recombinant GST (Lake Placid, NY) or albumin (Sigma) were adsorbed onto coverglass-bottom 96-well plates (Nunc, Rochester, NY) overnight at 4°C. Recombinant GST standards were made by diluting stock recombinant GST (1 mg/mL) to 10 μg/mL with PBS and serially diluting with PBS. At the same time, GST- FNIII$_{9\text{-}10}$ at 4 mg/mL was serially diluted with one part GST- FNIII$_{9\text{-}10}$ and one part PBS, and these various dilutions were adsorbed onto the well plates. Albumin standards were made by serially diluting stock albumin (300 mg/mL) with PBS. Wells were washed three times with PBS to remove unbound ligand and incubated with blocking buffer (1× PBS, 3% nonfat dry-milk) for 1 h at 37°C. After washing three times with PBS, substrates were incubated with rabbit anti-GST (70 ng/mL) (Sigma) or horseradish peroxidase–conjugated rabbit antialbumin (1:2500 dilution) (MP Biomedicals, Irvine, CA) for 1 h at 37°C. Wells incubated with anti-GST primary antibody were washed and further reacted with an appropriate horseradish peroxidase–conjugated goat antirabbit antibody (1:40,000) (Sigma) for 1 h at 37°C. Sigma-FAST OPD tablets (Sigma) were used according to the manufacturer's protocol as a substrate for the detection of peroxidase activity. The color reaction was developed for 30 min and absorbance read at 450 nm on a multi-well plate reader. The absorbance reading of the GST-FNIII$_{9\text{-}10}$-ANC was used to calculate the concentration of GST-FNIII$_{9\text{-}10}$ required to obtain an equivalent level of GST-FNIII$_{9\text{-}10}$ adsorbed using linear regression with the standard curve of GST-FNIII$_{9\text{-}10}$ absorbances. The levels of GST-FNIII$_{9\text{-}10}$ conjugated to ANC were obtained using linear regression using a standard curve of recombinant GST absorbances. Values for GST-FNIII$_{9\text{-}10}$ conjugated to the nanocarrier were normalized to albumin. To examine the role of mobility of our ligand through differential presentation, ligand and ligand–nanocarrier were immobilized to the surface using oxygen plasma pretreatment (March Plasma Inc, 60 s, 50 W, 670 mTorr oxygen) before ligand and ligand–nanocarrier deposition. Isotherms were established as described above.

ELISAs were also conducted to examine exposure of GST-FNIII$_{9\text{-}10}$ cell-binding domains as a function of ligand nanodisplay for passively adsorbed and immobilized substrates. Equivalent amounts of GST-FNIII$_{9\text{-}10}$ derived from GST ELISA isotherms were adsorbed on maxisorp 96-well plates overnight at 4°C. The surfaces were washed and blocked for 1 h at 37°C. Substrates were washed again and incubated with the primary antibody specific for the cell-binding domain in fibronectin (Clone 3E3; Chemicon International, Temecula, CA) for 1 h, followed by 1 h incubation with horseradish peroxidase–conjugated goat antimouse immunoglobulin (Ig)G (Sigma). Peroxidase activity was detected as described above.

Cell culture

Human foreskin fibroblasts were kindly provided by Patricia Simpson-Haidaris (University of Rochester, Rochester, NY). Fibroblasts were cultured in McCoy's 5 A medium (Invitrogen, Chicago, IL) supplemented with 1% penicillin/streptomycin (Biowhitaker, Walkersville, MD), 2 mM L-glutamine (Invitrogen), and 10% fetal bovine serum. For all assays, fibroblasts were washed with PBS, and medium was replaced with serum-free medium supplemented with the above supplements.

Imaging and semi-quantitative analysis of fibronectin matrix assembly

Matrix assembly was analyzed as a function of ligand carrier size and ligand density. Substrates with equal levels of ligand but differential presentation were adsorbed in 8-well Labtek chamber slides overnight at 4°C. Substrates were then washed generously with PBS and blocked with bovine serum albumin (BSA) for 1 h at 37°C. To isolate the serum-independent matrix assembly behavior of cells, fibroblasts were serum-starved 12 h before trypsinization and re-plated at a density of 35,000 cells per well in serum-free medium. Cells were then cultured for 24 h at 37°C with 5% carbon dioxide (CO_2). After 24 h of incubation, medium was removed, and substrates were washed with Dulbecco's PBS (DPBS) with calcium and magnesium. Cells were fixed with 1% formaldehyde for 9 min and washed with DPBS with calcium and magnesium. Cells were permeabilized with Triton-X 100 for 15 min, washed with DPBS with calcium and magnesium, and blocked with 1% BSA for 1 h at 37°C. Substrates were washed, and primary antibody IST-4 (Sigma) for fibronectin that binds to the 5th type III repeat of human plasma fibronectin was incubated at a 1:100 dilution in PBS overnight at 4°C. Substrates were washed and incubated with fluorescein isothiocyanate (FITC)-conjugated donkey antimouse IgG (Jackson Immunolabs, West Grove, PA) at a 1:200 dilution for 30 min at room temperature and were then washed and incubated with Texas-red phalloidin (Molecular Probes, Eugene, OR) for 20 min at room temperature. Substrates were washed and stored at 4°C until image acquisition. Images were acquired using a Leica TCS SP/2 confocal microscope with a 63× objective, zoom 1.

For conditions eliciting the highest levels of matrix assembly, substrates were plasma treated with 60% oxygen and 670 mTorr pressure with a plasma generator (March Plasma Systems, Concord, CA), and ligand was immediately deposited on treated substrates. The effect of medium presentation of ligand, as opposed to surface-adsorbed ligand, was examined by seeding cells on Labtek chamber slides for 2 h and then adding ligand-ANC to the medium. Cells were

then cultured for 24 h at 37°C with 5% CO_2. The effect of serum on matrix assembly for certain conditions was examined by culturing cells on substrates as described above without serum deprivation. As a control, whole-length mouse fibronectin (Innovative Research, Southfield, MI) was adsorbed at 10 μg/mL overnight at 4°C, and fibroblasts were seeded in serum-free medium.

Quantitation of fibronectin matrix assembly

The extent of assembly of cell-derived fibronectin matrix was quantified using ELISA. Substrate conditions where the most amount of matrix assembly was visualized after 24 h in culture were prepared as described above, along with the corresponding immobilized substrate conditions and unfunctionalized carriers. At the same time, a standard curve of whole-length fibronectin, ranging from 0 to 10 μg/mL diluted 10 times with PBS was adsorbed in triplicate. Cells were deposited on substrates for 24 h at 37°C with 5% CO_2 and washed three times at the end of the incubation period. Cells were lyzed as previously described[27] using lysis buffer composed of 8 mM disodium hydrogen phosphate dodecahydrate at pH 9.6 and 1% NP-40 for 15 min at 37°C. The solution was then removed and replaced with fresh lysis buffer and the incubation continued for an additional 60 min. Substrates were then washed, and an ELISA was performed by blocking substrates and the standard curve with 1% BSA for 1 h at 37°C and washing it three times. Next, the primary antibody (IST-4) at a concentration of 1:1,000 was incubated at 37°C for 1 h and washed off, followed by incubation of the secondary antibody, goat antimouse conjugated with horseradish peroxidase at a concentration of 1:10,000 (Sigma) for 1 h at 37°C. Sigma-FAST OPD tablets (Sigma) were used according to the manufacturer's protocol as a substrate for the detection of peroxidase activity. The color reaction was developed for 30 min and absorbance read at 450 nm on a multi-well plate reader. The absorbance reading of the fibronectin standard curve (similarly based on the IST-4 binding activity) was used to determine an equivalent bulk concentration level of fibronectin assembled.

Cell attachment

To quantify cell attachment to ligand-ANC, 96-well nontissue culture dishes were passively coated overnight at 4°C with varying ligand densities and presentations as described above. Wells were washed with PBS and blocked with 1% BSA. After washing, fibroblasts were seeded at 25,000 cells/well and incubated for 1 h at 37°C with 5% CO_2. Substrates were washed with PBS to remove unbound cells. Adhered cells were quantified using the hexosaminidase assay.[33] Briefly, a substrate mixture composed of 1 part 0.5% Triton-X 100 and 1 part 7.5 mM β-nitrophenyl N-acetyl β-D glucosaminide (Sigma) in 0.1 M citrate buffer (pH 5.0) was added to each well and incubated for 90 min at 37°C. The reaction was terminated with a mixture of 50 mM glycine (Sigma) and 5 mM ethylenediaminetetraacetic acid (Sigma) (pH 10.4). The absorbance was read at 405 nm on a multi-well plate reader.

Cell morphology

Cell morphology was examined as a function of differential ligand presentation and nanocarrier size at two time points. Passively adsorbed substrates were prepared as described above. Fibroblasts that were serum deprived for 12 h were seeded in serum-free medium for 1 or 5 h at 37°C with 5% CO_2. Substrates were washed after the designated incubation time and fixed with 3.7% formaldehyde for 15 min at room temperature. Substrates were washed again and permeabilized with Triton-X 100 for 15 min at room temperature. Substrates were washed, blocked with 1% BSA for 15 min at room temperature, washed again, and stained with FITC phalloidin (Molecular Probes) for 20 min. Substrates were washed and stored at 4°C until image acquisition. Images were acquired with a Leica TCS SP/2 at 63×.

Displacement of Fnf—ANC during Fibroblast Contraction

The possible cell-engendered translocation of ligand-ANCs was tracked by encapsulating a fluorescent probe within the ANCs. Briefly, albumin was denatured as described above. Before the solution was stirred, 10 μg of Alexa Fluor 488 (Molecular Probes) was added to the solution. The solution was then stirred to create nanocarriers and processed as described above. Various sized functionalized nanocarriers were adsorbed onto substrates such that the fluorescently labeled nanocarriers were diluted 1:1000 with unlabeled functionalized nanocarriers. Substrates were then washed and fibroblasts seeded at 2800 cells/cm^2. Cells were incubated for 1 h at 37°C with 5% CO_2, and image acquisition was performed on a Carl Zeiss LSM410 microscope every 45 min. At each time point, a fluorescent image and a phase contrast image were acquired. Images were merged, and the distance traveled was calculated by tracking the mobile nanocarriers over 6 h of image acquisition. Only carriers that were located at the edge of the cell at the initial time-lapse sequence were tracked, ensuring that cell-bound carriers were considered. For each experiment and condition, at least 15 carriers were tracked, and carrier displacement per time was averaged.

Quantitation of force curves between cells and ligand-ANC substrates

The force of interaction between cells and ligand-ANCs was evaluated using atomic force microscopy operating in fluid immersion mode. Silicon nitride cantilevers (Veeco Metrology, Santa Barbara, CA) were incubated overnight at 4°C with the appropriate ligand-ANC solutions of variable ANC sizes and ligand concentrations (0 and 2.2 μg/cm^2). Functionalized cantilevers were then washed with PBS and

blocked with 1% BSA for 1 h at 37C and washed again with PBS. The presence of ANCs was confirmed separately using scanning electron microscopy (data not shown). Fibroblasts were seeded at a density of 2800 cells/cm^2 onto clean glass slides and incubated for 1 h at 37°C with 5% CO_2 in serum-free medium. The ligand-adsorbed cantilever tip was allowed to carefully approach the surface of the peripheral regions of individual fibroblasts while maintaining a constant force of 0.38 N/m using an atomic force microscope (Digital Instruments Nanoscope IIIa, Santa Barbara, CA) under tapping mode. A force curve between the ligand—ANC–adsorbed cantilever and the cell was generated by oscillating the tip at 1 Hz. As the tip oscillated, the cantilever deflection from the photodiode was monitored, generating a force curve between the ligand-ANC–adsorbed cantilever tip and the cell on the glass slide. The force curve was a plot of the cantilever deflection signal as a function of the voltage applied to the piezo tube. The force was calculated as $F = -kx$, where k is the force constant of the spring, and x is the distance from the control point in nanometers. Each condition was examined in triplicate, and for each condition, force curves were generated on three to five different cells.

Statistics

Each experiment was performed at least twice, and at least two replicate samples were analyzed in each experiment and then analyzed using analysis of variance (ANOVA). Significance criteria assumed a 95% confidence level ($p < 0.05$). Standard error around the mean is reported in the final data.

RESULTS

Characterization of the ANC substrates

Different sized ANCs were synthesized by adjusting the mixing time during self-assembly. Dynamic light-scattering data show that four distinct, relatively homogeneous populations of ANCs were fabricated and ranged in average diameter from 30 to 125 nm (Fig. 1A). Atomic force microscopy was previously used to validate the size measurements from dynamic light scattering and revealed a near-spherical geometry.[30] ANCs were functionalized with a protein composed of GST fused to the $III_{9\text{-}10}$ cell binding domain of fibronectin (termed Fnf). To quantify the amount of Fnf conjugated to ANCs, equivalent amounts of nanocarriers were adsorbed onto surfaces, and an ELISA was performed with an anti-GST antibody (Fig. 1B). The results show that, by varying the amount of protein reacted with a fixed mass of nanocarriers, three different ligand-ANC preparations of 2.2, 1.3, and 0.4 μg/cm^2 were established for each nanocarrier size based on surface area of the well (Fig. 1B). The density of the functionalized ligand on the surface of the well plate (the substrate) was not appreciably affected by the size of the nanocarrier but was largely influenced by the initial amount of ligand reacted with the nanocarrier. These isotherms for functionalized ligand-equivalents were normalized against albumin isotherms, quantified with an ELISA for ligand-ANCs adsorbed on surfaces and compared with a standard curve of albumin (Fig. 1C). ELISAs for cell-binding domain exposure indicated that exposure was not different on different-sized carriers (data not shown).

Fibronectin matrix assembly is larger on larger ANCs

Cell adhesion and cytoskeletal organization are required steps in matrix assembly. To determine the role of ligand density and presentation in this process, immunofluorescence was performed on cells plated on different ligand-ANCs. Using ANCs with the highest ligand density, we observed a correlation between numbers of assembled fibronectin fibrils and nanocarrier size; 100- and 125-nm ANCs supported fibril formation detectable by 24 h (Fig. 2A, left column), with more prominent fibronectin matrix fibrils after 48 h (Fig. 2A, middle column). On smaller carriers or on adsorbed Fnf alone, occasional short fibrils were detected, but most of the fibronectin staining appeared to be intracellular. To examine the influence of nanocarrier size and ligand concentration on cell-engendered nanocarrier mobilization, substrates were oxygen plasma treated before ligand-ANC seeding to immobilize the nanocarriers. The plasma treatment "activates" the surface by introducing oxygen moieties to the surface before ligand deposition. Once deposited, the differentially presented ligand is coupled to the surface.[34] Because the plasma treatment procedure declines with time if the added groups are not used,[35,36] protein was deposited within minutes of the treatment. Cells extended more membrane projections on immobilized nanocarriers, and fewer fibronectin fibrils were detected (Fig. 2A, right column). Fibril densities were more than 10 times greater on 100- and 125-nm carriers than on smaller ANCs. These results show that nanocarrier size is an important effector of fibronectin matrix assembly. At lower ligand densities, there was no detectable assembly of matrix regardless of ligand presentation, and fibrils were not seen on unfunctionalized ANCs or on control substrates adsorbed with whole-length mouse fibronectin (data not shown). We examined whether ligation of integrins to ligand-ANCs was sufficient to induce matrix assembly by supplementing the medium with ligand-ANC as opposed to adsorbing the ligand-ANC directly to the surface. Here, matrix assembly was not evident. Comparing matrix assembly using immunochemistry techniques on the assembled matrix by cells after 24 h in culture at the highest ligand loading with that on unfunctionalized carriers indicated a distinguishable difference in fibronectin assembled between different-sized carriers at the highest ligand loading (Fig. 2B). Analysis revealed a 22% increase of fibronectin matrix assembled.

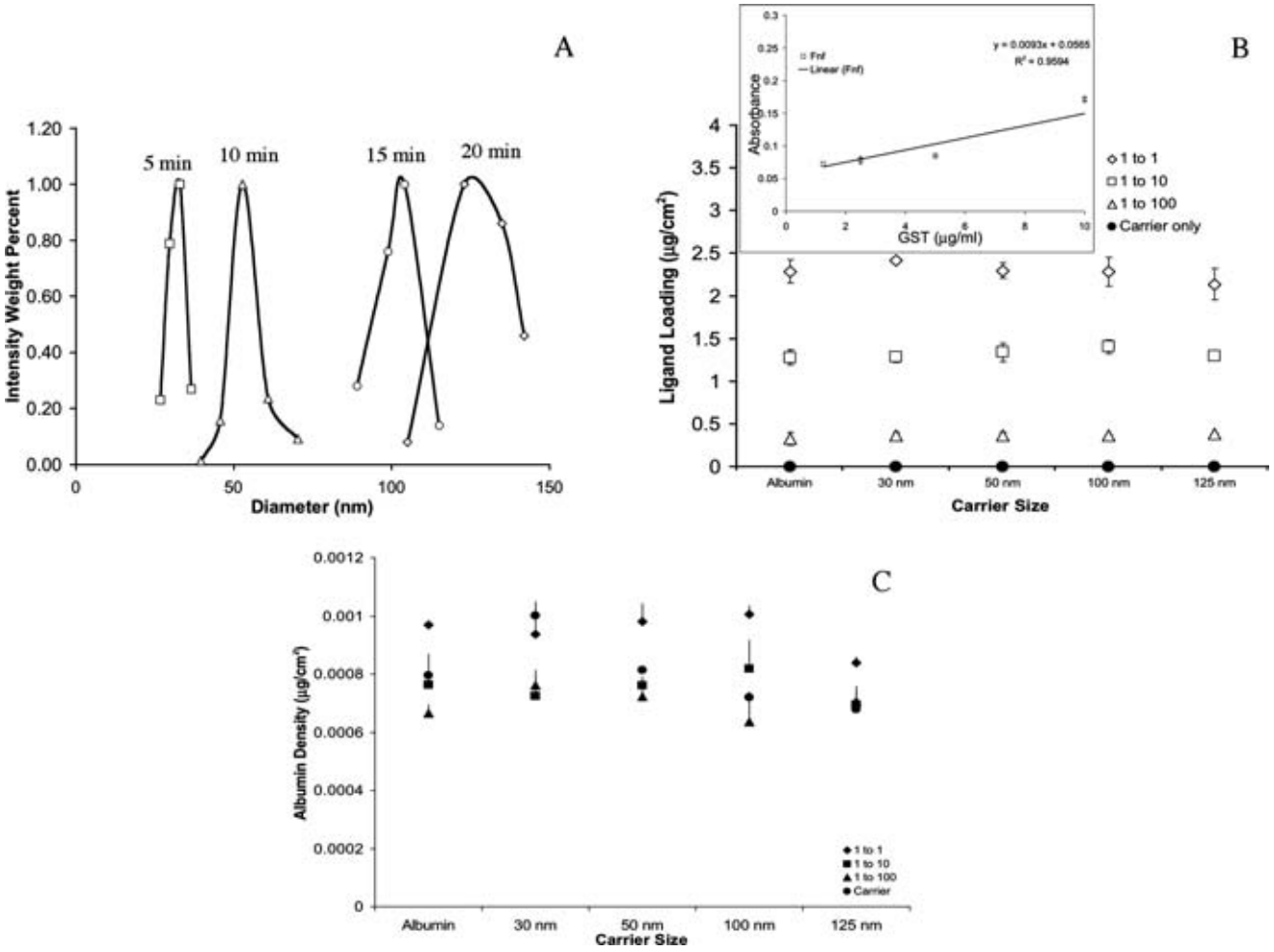

FIG. 1. (**A**) Albumin-derived nanocarriers (ANCs) were fabricated through self-assembly processes after denaturation via changes in pH and temperature. Sizes of nanocarriers at different mixing times were determined using dynamic light scattering. Inset is the average size of ANCs from three different batches. (**B**) ANCs are functionalized with ligands by reactin ANCs with cross-linker and reacting the ANCs that have been treated with cross-linker with ligand that had its amino group displaced and replaced with a thiol group as described in the text. The mass of ANCs was held constant, and increasing amounts of ligand were functionalized on various sized carriers. Substrates were adsorbed with ligand-ANCs at various loadings, with a standard curve for the ligand and then probed using enzyme-linked immunosorbent assay (ELISA) via antibody for glutathione-S-transferase. The amount of ligand conjugated to ANCs at each ratio was calculated by determining the concentration from the standard curve, multiplying by the volume added, and dividing by the area of the well plate. Error bars represent standard error around the mean. Ligand coverage increases with increasing amount of ligand reacted with ANCs. Inset: standard curve on which calculations are based for one experiment. (**C**) Ligand isotherms were normalized to albumin isotherms. Substrates were adsorbed with various sized nanocarriers and ligand loadings with a standard curve for albumin and were then probed with ELISA against albumin. Differentially sized carriers did not appreciably alter the net amount of albumin coverage on the surface. Unless stated, all results represent average of three experiments performed in duplicate with the standard error plotted around the mean.

Fibroblasts cultured on smaller-sized carriers (30 and 50 nm) and unfunctionalized carriers assembled negligible amounts of fibronectin.

Nanocarrier size controls cell attachment and morphology

To examine whether the nanoscale presentation of ligand could alter initial cell binding and attachment events, equal numbers of fibroblasts were seeded in parallel on substrates of three different ligand densities with different presentations (Fig. 3A). Cell attachment was greater with greater ligand density. For a specific ligand density, the highest degree of attachment was seen on the largest nanocarrier (125 nm). Significant attachment, but to a lesser degree, was also observed on the 100-nm nanocarrier and on the ligand-only substrate, both distinguishable from each other when analyzed using ANOVA. On 30- and 50-nm carriers, attachment was similarly low.

The effects of ligand presentation on cytoskeletal organization were examined by staining for F-actin at different time points (Fig. 3B). Cells on larger ligand-ANCs began

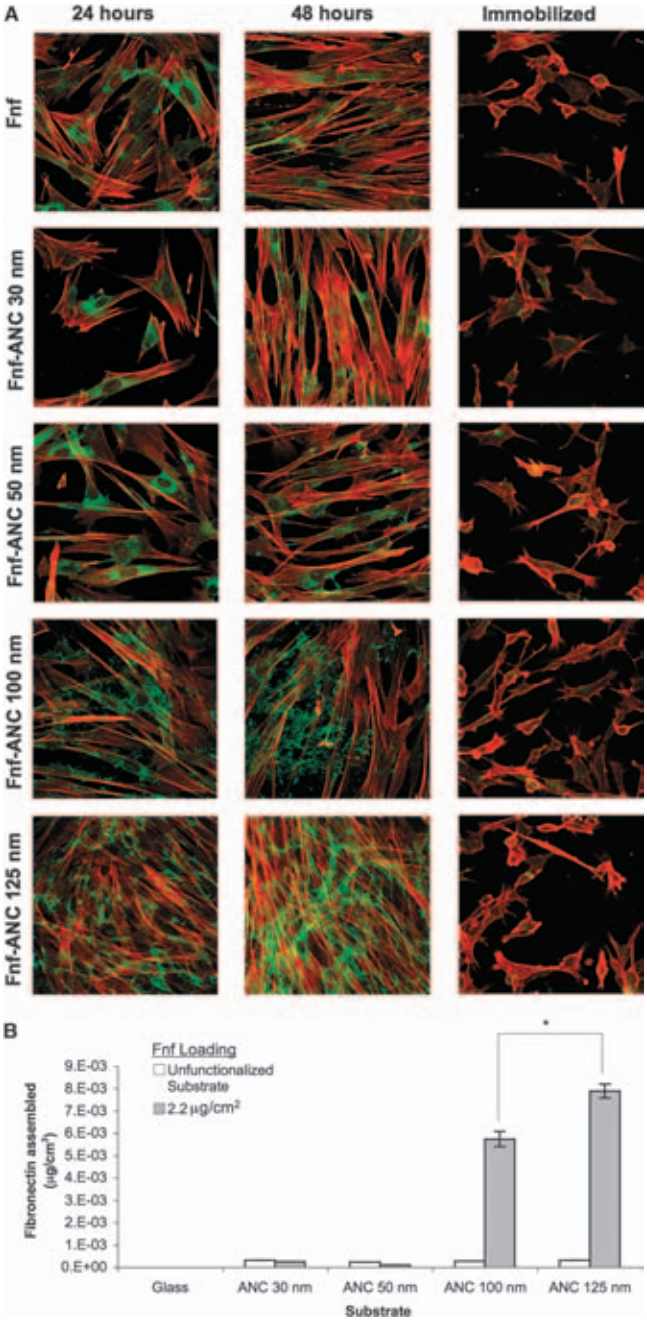

FIG. 2. Greater ligand concentration and albumin-derived nanocarrier (ANC) size promote the cell assembly of fibronectin matrix. (**A**) Human foreskin fibroblasts were serum-starved overnight and seeded on substrates with ligand at 2.2 μg/cm^2 for 24 h (left column) or 48 h (middle column). After the designated time point, cells were fixed, permeabilized, and processed for immunofluorescence. Matrix fibrils were visualized using a monoclonal mouse antihuman fibronectin epitope located within domain 5 of the type III repeats, followed by fluorescein isothiocyanate–conjugated secondary antibody. Cells were also stained for F-actin with Texas Red phalloidin. Longer culture time allowed cells seeded on smaller carriers to elongate and contract, yet matrix assembly still did not commence, whereas larger carriers not only assembled more matrix, but also became contracted. The influence of ligand-carrier mobility on matrix assembly was evaluated by immobilizing the carriers with plasma treatment before cell seeding (right column). Cells were cultured on substrates for 24 h and fixed, permeabilized, blocked, and stained for immunofluorescence as described above. Images were acquired at 63×, zoom 1. F-actin labeling with rhodamine-phalloidin reveals that cells were not as elongated on the immobilized carriers. Immunolabeling of fibronectin demonstrated that matrix assembly did not occur when carriers were not mobile. Bar = 20 μm. (**B**) Extent of matrix assembly was quantified using enzyme-linked immunosorbent assay (ELISA) techniques. Cells were cultured on substrates, as described in the text, with a standard curve of fibronectin, and lyzed to leave behind the assembled matrix. Substrates were then blocked and incubated with antihuman fibronectin for domain 5 of the type III repeats, followed by enzyme-linked secondary antibody. Values of ELISA absorbance were derived by back-calculating the concentration based on the standard curve of whole length fibronectin. *Statistical significance according to analysis of variance analysis when experiments were conducted in duplicate three times ($p < 0.05$). In summary, greater levels of fibronectin matrix was assembled on substrates with larger nanocarriers.

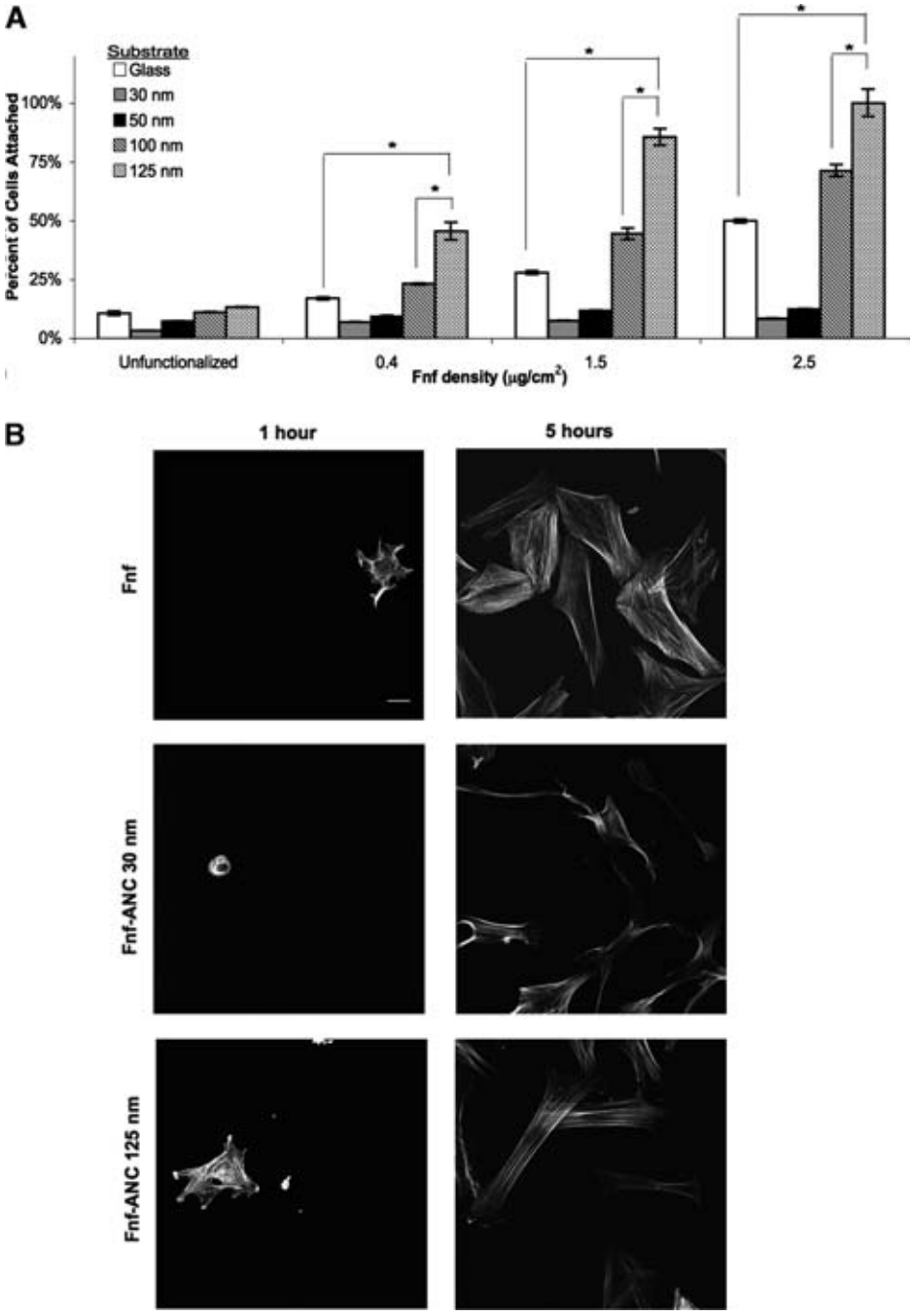

FIG. 3. Nanoscale presentation of ligand elicits differential early cell adhesion and morphogenesis. (**A**) Substrates with various sized albumin-derived nanocarriers (ANCs) and ligand densities were prepared as described in the text, and equal numbers of cells were seeded on surfaces with equal amounts of fibronectin fragments that were differentially presented to the cells as ligand adsorbed or via various sized ANCs. Cells were incubated for 1 h, unbound cells were washed, and the number of adherent cells was quantified using the hexosaminidase assay. The number of cells attached to each surface was normalized to the condition with the highest attachment (2.2 μg/cm^2 on 125 nm Fnf–ANC). Cell attachment was greater with larger ANC size and ligand density. Attachment was better on larger ANCs (100 nm and 125 nm) than on the fibronectin fragment alone. *Statistical significance according to analysis of variance when experiments were conducted in duplicate three times ($p < 0.05$). (**B**) Cell morphology was examined for fibroblasts cultured at the optimal ligand density for cell attachment (2.2 μg/cm^2) for 1 and 5 h. Cells were then washed, fixed, permeabilized, and stained with phalloidin. Images were acquired at 63×, zoom 1. Spreading occurred earlier on larger carriers (125-nm ANCs) than on smaller ones. By 5 h, cells had spread in all ligand-ANC conditions, but fibroblasts on larger ANCs were more elongated and exhibited more stress fibers. No attached cells were observed after 1 or 5 h of incubation, followed by rinsing, for the unfunctionalized substrate or the unfunctionalized nanocarriers (data not shown). Spreading on the fibronectin fragment was qualitatively comparable with that on the whole-length fibronectin (data not shown). Bar = 20 μm.

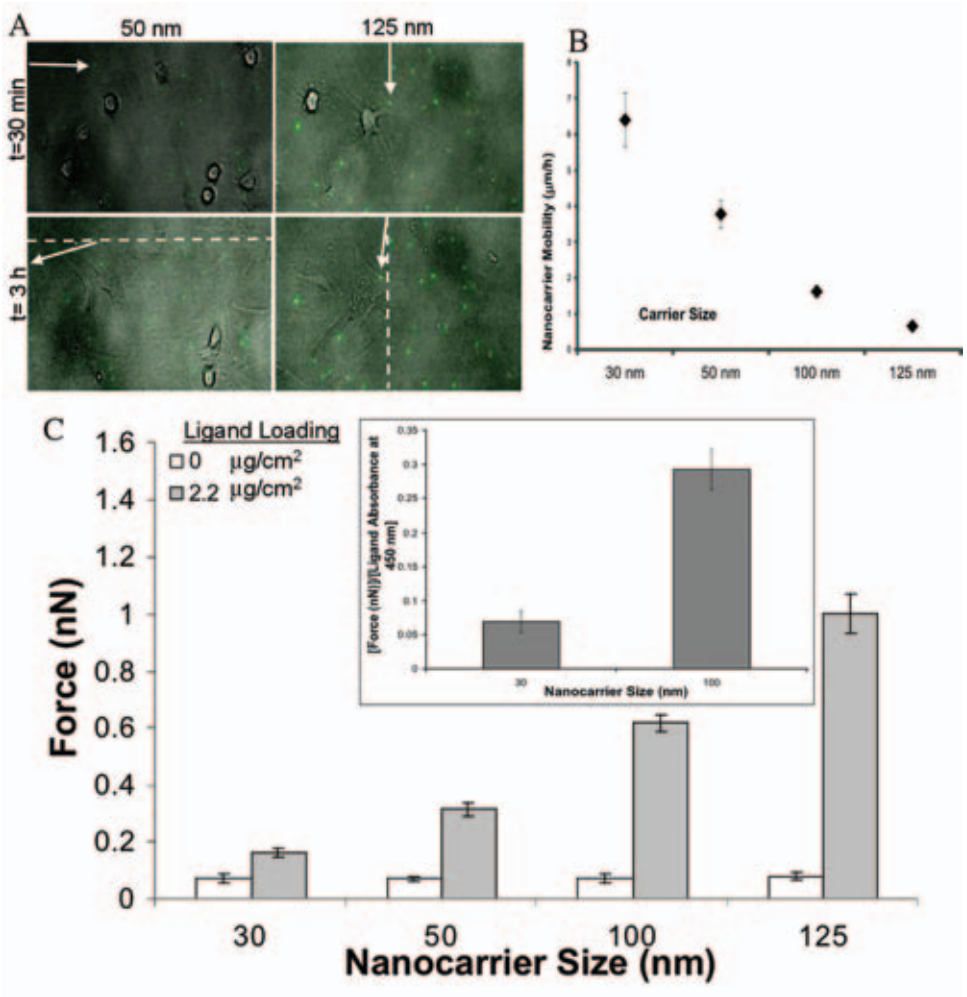

FIG. 4. The role of albumin-derived nanocarrier (ANC) size on matrix assembly. (**A**) To examine how ANC size can affect movement of ligand-ANCs, fluorescent ligand-ANCs were diluted with unlabeled ligand-ANCs and adsorbed as described in the text to visualize individual ligand-ANCs. Representative overlay images of fluorescent ligand-ANCs (green) and fibroblasts at two time points during the time lapse tracking on fluorescently labeled ANCs. Top row represents 30 min post-seeding with arrow pointing out one fluorescent ligand-ANC at an initial time point. Bottom row represents 3 h post-seeding with a dashed line to provide references for comparison relative to initial time point and arrow indicating the location of the fluorescent ligand-ANC after 3 h of incubation with cells. (**B**) Tracking and quantification of particle movements for the various conditions revealed that carrier mobility was lower with larger carrier size. Data represent the mean from three different experiments, with 15 carriers tracked from different cells per condition in each experiment. Error bars represent standard error. *Statistical significance according to analysis of variance analysis ($p < 0.05$). (**C**) Atomic force microscopy of differentially sized ligand-ANCs. To gain quantitative insights into the force required to displace ligand-ANCs of various sizes, various sized ligand-ANCs (30, 50, 100, and 125 nm) were functionalized to silicon nitride cantilevers by adsorbing overnight, and unbound ligand-ANCs were washed off. Force curves between derivatized cantilevers with a spring constant of 0.38 N/m and fibroblasts were generated in the fluid phase. As functionalized carrier size increased, the force between the cell and the cantilever also increased, indicating it was harder to disrupt the bond between the cell and the cantilever. No change in force was observed with unfunctionalized carriers. Overall, ANC size can influence detachment of ligand-ANCs from cantilevers adsorbed with ligand-ANCs. Color images available online at www.liebertpub.com/ten.

to exhibit stress fibers as early as 1 h postseeding. Cells cultured on ligand-adsorbed substrates had some filopodial projections after 1 h in culture, whereas those on smaller, functionalized carriers remained rounded with restricted spreading. When the culture time was extended to 5 h, cells on all substrates appeared well spread, with well-defined stress fibers, although cells on ligand-functionalized nanocarriers appeared somewhat more elongated. Cells plated on unfunctionalized controls did not attach. These results show that cell attachment and cytoskeletal organization occur more rapidly (within 1 h) on larger carriers than on smaller ones.

Variably sized ANCs exhibit differential cell-mediated mobility

Previous studies examining epithelial cell response to ANCs have demonstrated that the ligand–nanocarriers exhibit significant dynamics after cell binding.[30] Parallel time-lapse studies of the displacement rates of fluorescently labeled nanocarriers without plasma immobilization revealed that cells displaced smaller carriers further than larger ones over the first 6 h after seeding (Fig. 4A, B). Displacement rates (speed) varied about seven times between the smallest and largest ANCs. Transmitted images taken in parallel showed that fibroblasts on smaller functionalized carriers were round at 30 min but by 3 h began to spread and reached an elongated morphology (Fig. 4A). Cells on larger functionalized carriers were already spread at the first time point and appeared contracted and elongated by the end. Thus ligand-ANC mobility is inversely correlated with cell spreading and matrix assembly.

Variably sized ANCs require differential forces for cell-mediated mobilization

We hypothesized that nanocarrier size could modulate the degree of ligand-ANC translocation and that, to achieve translocation of larger ANCs, the cells must exert greater forces to overcome greater inertia from the larger carriers. To quantify the effect of carrier size on translocation of ligand-ANCs, silicon nitride cantilevers were functionalized with ligand-ANCs and brought into contact with fibroblasts that were cultured on glass slides. Force curves between various-sized ligand-ANCs at the highest ligand density and fibroblasts indicate that larger forces are generated in the cantilever during detachment between single adherent fibroblasts and the tips functionalized with larger ligand-ANCs than the forces between cells and smaller ligand-carriers (Fig. 4C). Unfunctionalized carriers exhibited small forces that were distinguishable from each other. Through tip-based ligand-specific ELISAs, we estimated that there is not a significant variation in ligand concentration on carriers of different sizes (30 and 100 nm), although different levels of ligands functionalized to differentially sized ANCs did not sensitively influence the force of ANC detachment from the tip (see inset in Figure 4C).

DISCUSSION

This study examined the role of nanoscale-engineered interfaces as a tool for regulating matrix assembly of fibronectin fibrils, a key step in the engineering of extracellular matrix. Our key findings are that the carrier size for ligand functionalization can modulate early cell binding and attachment events to the substrate, ligand density and nanocarrier size can dictate matrix assembly, and the mobility of the ligand-functionalized nanocarriers is an important determinant of matrix assembly.

Nanoscale substrates for presentation of adhesion ligand

We have previously reported on substrates based on ANCs to engineer cell motility and matrix assembly.[29,30] Albumin was chosen to create a family of various-sized nanocarriers because it is easily functionalized with the ligand of interest, is biodegradable *in vivo*, has a high level of biocompatibility, and allows effective exposure of adhesion ligands against a relatively inert background. Using immunosorbance techniques, we have demonstrated that nanocarrier size does not affect the concentration of ligand conjugated on differentially sized ANCs, measured in mass of ligand per unit area of the well, which depends solely on the amount of ligand in the initial reaction. Similarly, neither the presence of the ligand on the nanocarrier nor increasing ligand density on the nanocarrier altered the amount of albumin per unit area of the well.

By establishing adsorption isotherms, we could differentially control the presentation of the ligand on the ANC by determining the bulk concentrations of ligand and ligand-ANC required to have equivalent net concentrations. Matrix assembly studies were then conducted on surfaces with different ligand concentrations and nanocarrier sizes. To isolate the influence of the ligand presentation from ANC substrate on matrix assembly, experiments were conducted in a serum-free medium that supported comparable levels of cell viability as examined using ethidium homodimer labeling[37] (data not shown). Serum-supplemented media may contain lysophosphatidic acids, which would promote matrix assembly by inducing contraction, and soluble fibronectin.[24,25] Control experiments with 30- and 100-nm ligand-functionalized nanocarriers in serum containing medium reveal copious amounts of matrix assembly with indiscernible differences between the amounts of different-sized substrates (data not shown), further requiring the need to conduct studies of substrate-based approaches for matrix assembly in a serum-free system. In the serum-free environment, cells rely on the clustering of their integrins to the substrate to induce spreading and adhesion by activating focal adhesion kinase and other small Rho GTPases, including Rho.[38]

Matrix assembly can be modulated using ANC size, ligand density, and mobility

Our studies have demonstrated that, at the highest ligand concentrations, larger ligand-ANCs (>100 nm) promoted matrix assembly better than smaller ligand-ANCs and ligand-adsorbed substrates. Morphologically, fibroblasts appeared elongated and contracted on the larger-sized ligand-ANCs and were proximally located to each other, which is ideal for fibroblast-associated fibronectin fibrillogenesis.[25] Cells on smaller ligand-ANCs appeared well spread but were not as contracted. Time-lapse studies demonstrated slower cell spreading on small ANCs than on larger ligand-ANCs.

By 48 h, although cells on smaller ANCs appeared elongated and contracted, no appreciable matrix assembly was observed. However, cells on larger carriers produced even greater amounts of matrix. Theoretically, although matrix assembly experiments were conducted on substrates with equal net ligand coverage in the well, the actual coverage on the individual carrier could be different for each carrier, and this could be a factor in the lower levels of matrix assembly on smaller carriers. To address this possibility, we also functionalized smaller ANCs with larger concentrations of ligand, so the net ligand coverage on these carriers would be equivalent to the per-carrier loading on 100-nm carriers. Even with greater ligand coverage on smaller carriers, matrix assembly did not ensue (data not shown), suggesting that, although ligand concentration is an important factor, carrier size has a ''multiplier'' effect on matrix assembly.

These matrix assembly studies with equal amounts of ligand on differentially sized ANCs suggest that not just the nanoscale presentation of the ligand and ligand density, but also the size of the ANC can modulate cell-binding events and subsequent cell function. Cell attachment studies have showed that cell adhesion to larger ANCs was greater than that observed on smaller ANCs at all levels of ligand loading examined. Reports by our group and others affirm that cell attachment to ligands presented on substrates that promote integrin clustering also enhances cell attachment and adhesion strength.[29,30,39] When adhered, these cells produce and deposit fibronectin into the extracellular matrix.[40]

Because the cells could sequester our ligand-ANCs, we indirectly examined whether the mobility of ligand-ANCs was playing a role in matrix assembly. We immobilized ligand-ANCs on glass surfaces using oxygen plasma treatment as a control surface.[34] Our data showed that we needed to use a lower bulk concentration of ligand on immobilized substrates to obtain the same ligand density attained on passively adsorbed substrates, which was consistent with the literature.[41] Relatively equivalent exposure of the cell-binding domain of the fibronectin fragment ligand was observed on passively adsorbed and immobilized substrates (data not shown). The limited matrix assembly elicited on immobilized substrates indicated that it is likely that ligand-ANC mobility is a critical requirement for induction of matrix assembly.

Variably sized ANCs parallel substrates with varying degrees of compliance

We hypothesized that carrier size influenced fibroblast-mediated matrix assembly on various-sized ligand-ANCs because of different degrees of mobility, effectively acting similarly to varying degrees of substrate compliance that cause altered levels of cytoskeletal tension. Functionalized nanoscale carrier substrates offer an advantage by permitting greater ligand mobility,[42] which mimics the extracellular matrix features *in vivo*.[43] Previous studies have reported that the compliance of the dimensionality and rigidity of the substrate can govern fibroblast matrix assembly.[27,44] In the present work, we detected less movement of larger carriers than of smaller carriers with equal amounts of ligand. Thus, we posit that the cells generate intracellular forces to overcome the greater inertial mass and the increased frictional forces of the carrier with the underlying substrates, both entities being functions of the volume (or size) of the carrier.

Depending on the resistance offered by the nanocarrier-based substrate, the increase in cellular contractile force due to the mass of the nanocarriers can generate tension in the cytoskeleton in a manner that, for a specified ligand density, is dependent on the size of the nanocarrier. Similar to cells on stiff gels, this increase in cytoskeletal tension would induce earlier spreading by fibroblasts cultured on larger carriers.[45–47] Alternatively, when fibroblasts are cultured on smaller carriers, which we parallel to compliant substrates, the force required to move the carriers is less, and the carriers are easier for the fibroblasts to sequester. Because less tension is generated in the cell, the traction necessary to initially spread is not provided, delaying cell spreading and subsequent changes necessary for matrix assembly. There are some nonspecific adhesive forces between the glass substrate and the nanocarriers that the cell needs to overcome to translocate ligand-nanocarriers, but the inertial mass of the nanocarrier plays a greater role in mediating matrix assembly. Control studies in which ligand-functionalized nanocarriers were medium presented instead of adsorbed on the glass further support this; if nanocarrier size alone mediated matrix assembly, then there would have been matrix assembly in this presentation method. Our system permits matrix assembly due to substrate-based tractional forces as a function of nanocarrier size, but the nanoscale organization of the ligand is also playing a role in matrix assembly by potentially permitting necessary integrin clustering that is normally achieved in a three-dimensional system found *in vivo*. Because matrix assembly did not occur on nanocarrier-deficient ligand-adsorbed substrates as well as substrates with smaller nanocarriers, integrin clustering should also be recognized as a plausible mediator of matrix assembly on these substrates.

Our studies using atomic force microscopy further support the notion that nanocarrier size scale may sensitively influence the development of cell traction forces needed to mobilize the carriers. In these studies, we let cantilever-adsorbed ligand-ANCs of different sizes adhere to individual cells and then measured the forces required to mobilize them from the cantilever tip. These studies indicated that the detachment forces between the cell and the ligand-ANC–adsorbed cantilever were significantly greater for larger ANCs in contact with fibroblasts than smaller ones. We believe that the ''snap-off'' forces reflect the detachment of the ligand-ANC from the tip as opposed to detachment of the ligand-ANC from the cell. The latter requires far greater forces ($\sim$500 nN), as reported by others,[48] than those that we report. Furthermore, using *in situ* immunocytochemistry,

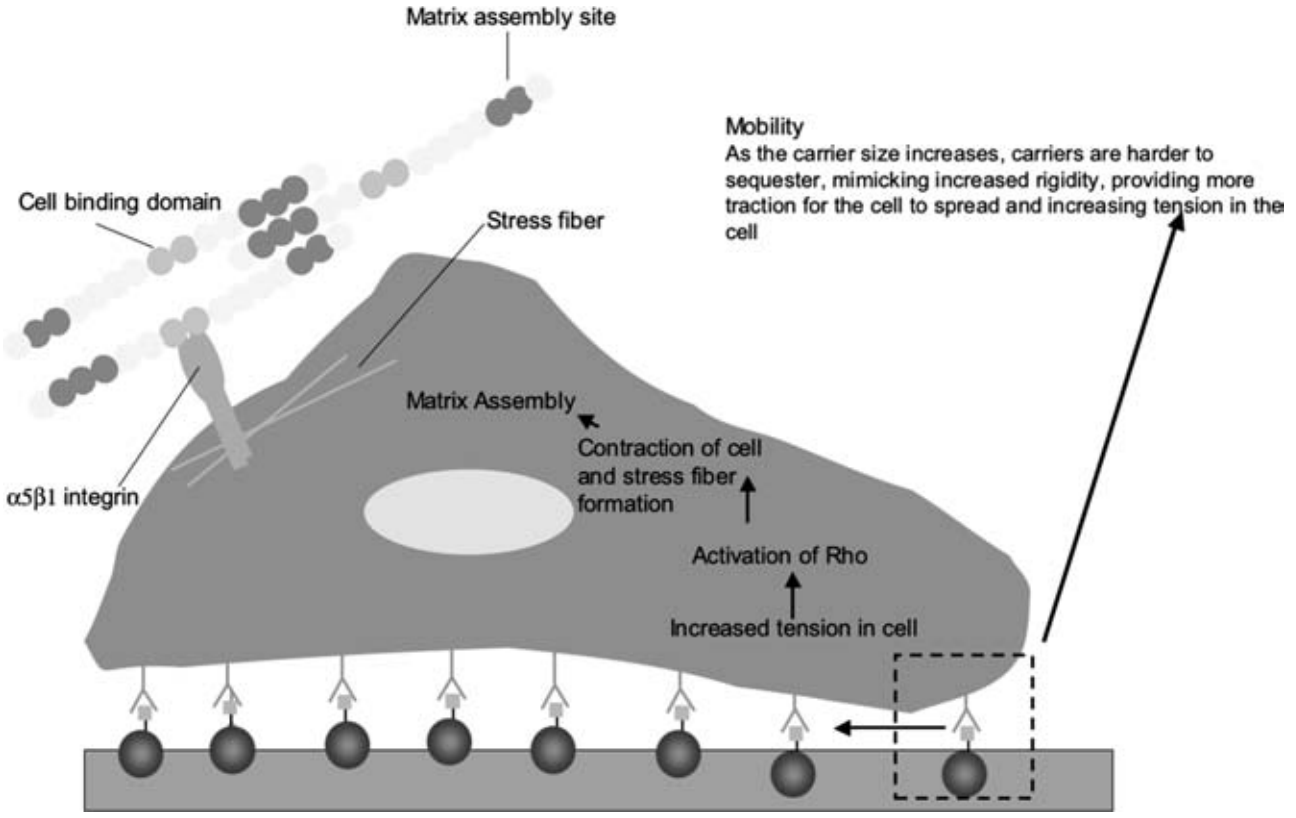

FIG. 5. Proposed mechanism of enhanced matrix assembly. When fibroblasts were cultured on dynamic interfaces, such as ligand–albumin-derived nanocarriers (ANCs), the ligand density and nanocarrier geometry mediated matrix assembly. Larger nanocarriers were difficult to sequester because of greater mass inertia, greater frictional forces, and greater resistance to displacement through fluid medium. As the cell attempts to move the carrier, tension is generated in the cell, which could lead to activation of Rho. Tension induced fibroblast contraction and formation of stress fibers, which allowed $\alpha5\beta1$ that was bound to soluble fibronectin to translocate across the stress fibers and elongate the molecule of fibronectin, exposing otherwise encrypted domains of fibronectin and permitting other fibronectin molecules to bind to it to create fibrils.

we estimated that the ligand coverage on the tip of the cantilever for different-sized carriers was fairly comparable (data not shown), indicating that ANC size, and not ligand concentration, was a key determinant of the cell detachment forces.

Working model for matrix assembly on ligand-ANC substrates

We offer a simple working molecular model that captures the observations of our study within the context of the emerging literature on cell-mediated matrix assembly (Fig. 5). *In vivo*, extracellular matrix components are highly elastic and undergo continual movement in response to cell–matrix interactions,[49] and cellular responses to mechanical signals can occur in seconds to minutes.[50] Similar to the *in vivo* situation, by engineering a system to present a truncated fragment of fibronectin that strategically promotes the binding of the $\alpha5\beta1$ integrin in a manner that allows integrin clustering, we allow cytoskeletal tension[51] and actin-dependent translocation of integrins involved in matrix assembly.[52] Upon ligation of this integrin to this region of fibronectin, Rho is activated,[53] which assists in the formation of stress fibers and contraction of the cell. When the $\alpha5\beta1$ integrin binds to soluble fibronectin, it translocates across stress fibers and transmits cytoskeletal-generated tension to the fibronectin,[54] which stretches the fibronectin molecule to expose cryptic sites necessary for matrix assembly.[55] Other ligands that affect early binding events or act synergistically could be similarly incorporated. Mobile nanoscale carriers also promote cell contraction and subsequent matrix assembly, and ligand density and carrier size can be tuned to optimize cell-binding events, beginning with cell spreading and ending with the specific desired phenotypic behavior. Although the proposed system uses an interface that has mobile nanocarriers on glass, our system is relevant to tissue engineering because it offers an understanding of a mechanism to drive matrix assembly with a substrate-based approach over a biochemical method. A novel feature of our system is that matrix assembly can still occur in an environment in which soluble fibronectin is not readily available. The use of mobile nanocarriers appears

to promote synthesis and secretion of soluble fibronectin, which can be exploited as a basis to engender active matrix assembly in wound environments of the skin as well in three-dimensional tissue-engineering scaffolds.

ACKNOWLEDGMENTS

This research was funded by National Science Foundation (NSF) NIRT0609000 and DGE0333196, Rutgers University Academic Excellence Award, and National Institutes of Health (NIH) EB001046 (PVM). The authors gratefully acknowledge ongoing scientific collaboration with Professor Jean E. Schwarzbauer of Princeton University. RIS was supported by an NIH Biotechnology Training Fellowship and an NSF IGERT Fellowship. The technical assistance of Nicolette Wangler from Princeton University with Fnf purification and Thomas Gentzel, a Rutgers ISURF Summer Fellow and Rutgers Undergraduate Research Fellow, with cell culture and image analysis are greatly appreciated. The editorial guidance of María Pía Rossi, an NIH Tissue Engineering Postdoctoral fellow, is gratefully acknowledged.

REFERENCES

1. Singer AJ, Clark RA. Cutaneous wound healing. N Engl J Med **341,** 738, 1999.
2. Hosgood G. Stages of wound healing and their clinical relevance. Vet Clin North Am Small Anim Pract **36,** 667, 2006.
3. Clark RA. Fibrin and wound healing. Ann N Y Acad Sci **936,** 355, 2001.
4. Broughton G. 2nd, Janis JE, Attinger CE, The basic science of wound healing. Plast Reconstr Surg **117 (7 Suppl),** 12S, 2006.
5. Corbett SA, Schwarzbauer JE. Fibronectin-fibrin cross-linking: a regulator of cell behavior. Trends Cardiovasc Med **8,** 357, 1998.
6. Hinz B, Gabbiani G. Mechanisms of force generation and transmission by myofibroblasts. Curr Opin Biotechnol **14,** 538, 2003.
7. Midwood KS, Williams LV, Schwarzbauer JE. Tissue repair and the dynamics of the extracellular matrix. Int J Biochem Cell Biol **36,** 1031, 2004.
8. Ghosh K, Ren XD, Shu XZ, Prestwich GD, Clark, RA. Fibronectin functional domains coupled to hyaluronan stimulate adult human dermal fibroblast responses critical for wound healing. Tissue Eng **12,** 601, 2006.
9. Mimura Y, Ihn H, Jinnin M, Asano Y, Yamane K, Tamaki K. Epidermal growth factor induces fibronectin expression in human dermal fibroblasts via protein kinase C delta signaling pathway. J Invest Dermatol **122,** 1390, 2004.
10. Thompson HG, Mih, JD, Krasieva TB, Tromberg BJ, George SC. Epithelial-derived TGF-{beta}2 modulates basal and wound healing subepithelial matrix homeostasis. Am J Physiol Lung Cell Mol Physiol **291,** L1277, 2006.
11. Broughton G. 2nd, Janis JE, Attinger CE. Wound healing: an overview. Plast Reconstr Surg **117 (7 Suppl),** 1e-S, 2006.
12. Li J, Zhang YP, Kirsner RS. Angiogenesis in wound repair: angiogenic growth factors and the extracellular matrix. Microsc Res Tech **60,** 107, 2003.
13. Riedel K, Riedel F, Goessler UR, Holle G, Germann G, Sauerbier M. Current status of genetic modulation of growth factors in wound repair. Int J Mol Med **17,** 183, 2006.
14. Rumalla VK, Borah GL. Cytokines, growth factors, and plastic surgery. Plast Reconstr Surg **108,** 719, 2001.
15. Roy P, Petroll WM, Cavanagh HD, Jester JV. Exertion of tractional force requires the coordinated up-regulation of cell contractility and adhesion. Cell Motil Cytoskeleton **43,** 23, 1999.
16. Mao Y, Schwarzbauer JE. Fibronectin fibrillogenesis. A cell-mediated matrix assembly process. Matrix Biol **24,** 389, 2005.
17. Aota S, Nomizu M, Yamada KM. The short amino acid sequence Pro-His-Ser-Arg-Asn in human fibronectin enhances cell-adhesive function. J Biol Chem **269,** 24756, 1994.
18. Danen EH, Aota S, van Kraats AA, Yamada KM, Ruiter DJ, van Muijen GN. Requirement for the synergy site for cell adhesion to fibronectin depends on the activation state of integrin alpha 5 beta 1. J Biol Chem **270,** 21612, 1995.
19. Main AL, Harvey TS, Baron M, Boyd J, Campbell ID. The three-dimensional structure of the tenth type III module of fibronectin: an insight into RGD-mediated interactions. Cell **71,** 671, 1992.
20. Leahy DJ, Aukhil I, Erickson HP. A crystal structure of a four-domain segment of human fibronectin encompassing the RGD loop and synergy region. Cell **84,** 155, 1996.
21. Zhong C, Chrzanowska-Wodnicka M, Brown J, Shaub A, Belkin AM, Burridge K. Rho-mediated contractility exposes a cryptic site in fibronectin and induces fibronectin matrix assembly. J Cell Biol **141,** 539, 1998.
22. Singer II. Association of fibronectin and vinculin with focal contacts and stress fibers in stationary hamster fibroblasts. J Cell Biol **92,** 398, 1982.
23. Mautner V, Hynes RO. Surface distribution of LETS protein in relation to the cytoskeleton of normal and transformed cells. J Cell Biol **75,** 743, 1977.
24. Zhang Q, Magnusson MK, Mosher DF. Lysophosphatidic acid and microtubule-destabilizing agents stimulate fibronectin matrix assembly through Rho-dependent actin stress fiber formation and cell contraction. Mol Biol Cell **8,** 1415, 1997.
25. Zhang Q, Checovich WJ, Peters DM, Albrecht RM, Mosher DF. Modulation of cell surface fibronectin assembly sites by lysophosphatidic acid. J Cell Biol **127,** 1447, 1994.
26. Chiquet M, Renedo AS, Huber F, Flück M. How do fibroblasts translate mechanical signals into changes in extracellular matrix production? Matrix Biol **22,** 73, 2003.
27. Mao Y, Schwarzbauer JE. Stimulatory effects of a three-dimensional microenvironment on cell-mediated fibronectin fibrillogenesis. J Cell Sci **118,** 4427, 2005.
28. Cukierman E, Pankov R, Stevens DR, Yamada KM. Taking cell-matrix adhesions to the third dimension. Science **294,** 1708, 2001.
29. Pereira M, Sharma RI, Penkala R, Gentzel TA, Schwarzbauer JE, Moghe PV. Engineered cell-adhesive nanoparticles nucleate extracellular matrix assembly. Tissue Eng **13,** 567, 2007.
30. Sharma RI, Pereira M, Schwarzbauer JE, Moghe PV. Albumin-derived nanocarriers: substrates for enhanced cell adhesive ligand display and cell motility. Biomaterials **27,** 3589, 2006.

31. Takeoka S, Teramura Y, Okamura Y, Handa M, Ikeda Y, Tsuchida E. Fibrinogen-conjugated albumin polymers and their interaction with platelets under flow conditions. Biomacromolecules **2,** 1192, 2001.
32. Takeoka S, Teramura Y, Ohkawa H, Ikeda Y, Tsuchida E. Conjugation of von Willebrand factor-binding domain of platelet glycoprotein Ib alpha to size-controlled albumin microspheres. Biomacromolecules **1,** 290, 2000.
33. Landegren U. Measurement of cell numbers by means of the endogenous enzyme hexosaminidase. Applications to detection of lymphokines and cell surface antigens. J Immunol Meth **67,** 379, 1984.
34. Favia P, d'Agostino R. Plasma treatments and plasma deposition of polymers for biomedical applications. Surface Coatings Technol **98,** 1102, 1998.
35. Schmalenberg KE, Buettner HM, Uhrich KE. Microcontact printing of proteins on oxygen plasma-activated poly (methyl methacrylate). Biomaterials **25,** 1851, 2004.
36. Yang J, Wan Y, Yang J, Bei J, Wang S. Plasma-treated, collagen-anchored polylactone: Its cell affinity evaluation under shear or shear-free conditions. J Biomed Mater Res A **67,** 1139, 2003.
37. Imbert D, Cullander C. Assessment of cornea viability by confocal laser scanning microscopy and MTT assay. Cornea **16,** 666, 1997.
38. Lehnert D, Wehrle-Haller B, David C, Weiland U, Ballestrem C, Imhof BA, Bastmeyer M. Cell behaviour on micropatterned substrata: limits of extracellular matrix geometry for spreading and adhesion. J Cell Sci **117,** 41, 2004.
39. Maheshwari G, Brown G, Lauffenburger DA, Wells A, Griffith LG. Cell adhesion and motility depend on nanoscale RGD clustering. J Cell Sci **113,** 1677, 2000.
40. Sottile J, Hocking DC, Swiatek PJ. Fibronectin matrix assembly enhances adhesion-dependent cell growth. J Cell Sci **111,** 2933, 1998.
41. Yang J, Bei J, Wang S. Enhanced cell affinity of poly (D,L-lactide) by combining plasma treatment with collagen anchorage. Biomaterials **23,** 2607, 2002.
42. Choquet D, Felsenfeld DP, Sheetz MP. Extracellular matrix rigidity causes strengthening of integrin-cytoskeleton linkages. Cell **88,** 39, 1997.
43. Katz BZ, Zamir E, Bershadsky A, Kam Z, Yamada KM, Geiger B. Physical state of the extracellular matrix regulates the structure and molecular composition of cell-matrix adhesions. Mol Biol Cell **11,** 1047, 2000.
44. Beningo KA, Dembo M, Wang YL. Responses of fibroblasts to anchorage of dorsal extracellular matrix receptors. Proc Natl Acad Sci U S A **101,** 18024, 2004.
45. Engler A, Bacakova L, Newman C, Hategan A, Griffin M, Discher D. Substrate compliance versus ligand density in cell on gel responses. Biophys J **86 (1 Part 1),** 617, 2004.
46. Jiang G, Huang AH, Cai Y, Tanase M, Sheetz MP. Rigidity sensing at the leading edge through alphavbeta3 integrins and RPTPalpha. Biophys J **90,** 1804, 2006.
47. Flanagan LA, Ju YE, Marg B, Osterfield M, Janmey PA. Neurite branching on deformable substrates. Neuroreport **13,** 2411, 2002.
48. Yamamoto A, Mishima S, Maruyama N, Sumita M. Quantitative evaluation of cell attachment to glass, polystyrene, and fibronectin- or collagen-coated polystyrene by measurement of cell adhesive shear force and cell detachment energy. J Biomed Mater Res **50,** 114, 2000.
49. Sivakumar P, Czirok A, Rongish BJ, Divakara VP, Wang YP, Dallas SL. New insights into extracellular matrix assembly and reorganization from dynamic imaging of extracellular matrix proteins in living osteoblasts. J Cell Sci **119,** 1350, 2006.
50. Vogel V, Sheetz M. Local force and geometry sensing regulate cell functions. Nat Rev Mol Cell Biol **7,** 265, 2006.
51. Geiger B, Bershadsky A. Exploring the neighborhood: adhesion-coupled cell mechanosensors. Cell **110,** 139, 2002.
52. Kawakami K, Tatsumi H, Sokabe M. Dynamics of integrin clustering at focal contacts of endothelial cells studied by multimode imaging microscopy. J Cell Sci **114,** 3125, 2001.
53. Danen EH, Sonneveld P, Brakebusch C, Fassler R, Sonnenberg A. The fibronectin-binding integrins alpha5beta1 and alphavbeta3 differentially modulate RhoA-GTP loading, organization of cell matrix adhesions, and fibronectin fibrillogenesis. J Cell Biol **159,** 1071, 2002.
54. Pankov R, Cukierman E, Katz BZ, Matsumoto K, Lin DC, Lin S, Hahn C, Yamada KM. Integrin dynamics and matrix assembly: tensin-dependent translocation of alpha (5) beta (1) integrins promotes early fibronectin fibrillogenesis. J Cell Biol **148,** 1075, 2000.
55. Baneyx G, Baugh L, Vogel V. Fibronectin extension and unfolding within cell matrix fibrils controlled by cytoskeletal tension. Proc Natl Acad Sci U S A **99,** 5139, 2002.

Address reprint requests to:
Prabhas V. Moghe, Ph.D.
Rutgers University
599 Taylor Road
Piscataway, NJ 08854

E-mail: moghe@rci.rutgers.edu

Received: September 4, 2007
Accepted: January 18, 2008